J. Geophys. 44, 441–471, 1978

Journal of Geophysics

# Simple Plate Models of Mantle Convection

F. Richter[1] and D. McKenzie[2]

[1] Department of the Geophysical Sciences, The University of Chicago, Chicago, Ill, 60637, USA
[2] Department of Geodesy and Geophysics, Cambridge University, Madingley Rise, Madingley Road, Cambridge CB3 OEZ, England

**Abstract.** A simple convective model that can maintain observed plate motions consists of a viscous upper mantle of uniform density overlain by denser rigid plates. In the absence of density differences within the upper mantle the viscous stresses exerted by the flow are easily obtained and demonstrate that the buoyancy forces associated with plate creation and destruction can maintain plate motions. A model having a uniform viscosity upper mantle is, however, unsatisfactory because it predicts gravity and residual depth anomalies two orders of magnitude larger than those observed. This problem can be overcome by introducing a thin low viscosity layer beneath the plates. The resulting model is then similar to that proposed by Forsyth and Uyeda and by Chapple and Tullis despite a very different approach. This agreement suggests that the energetics of plate motion are now understood in outline. The model cannot, however, account for the existence of the longwavelength gravity anomalies which are not associated with plate motions.

**Key words**: Plate dynamics – Mantle convection – Mantle viscosity.

## 1. Introduction

Though the kinetic description of the earth's surface motion has been generally accepted, there is much less agreement about how the motions are maintained. The dynamic problem consists of two separate but related questions: How does the mantle convert heat into mechanical work to maintain the observed plate motions, and why is the large-scale flow of which the plate motions form part stable to smaller scale motions? The first of these two questions is the simpler, and it is with it that this paper will be principally concerned. All the forces which we will consider arise from thermal convection: Heat is transported upward by hot, less dense, material rising to replace denser, colder material. However, the form the motion takes does not resemble Rayleigh-Benard con-

0340-62X/78/0044/0441/$06.20

vection. The dimensions and relative velocities of the plates are known by direct observation, and simple models for the thermal structure of ridges and sinking slabs account for a considerable variety of geophysical observations. If all other buoyancy forces are ignored it is straightforward to use this information to calculate the work supplied by the rigid plate motions themselves. This is the simple model we consider below. Though it is likely that the buoyancy forces near ridges and trenches provide an important part of the energy required to maintain the flow, exactly how important a part is not yet clear. It seems unlikely that the only buoyancy forces in the mantle are those which result from the temperature contrast between the sinking slabs and the surrounding mantle, and the corresponding forces at ridges. For a variety of reasons (Richter, 1973b; McKenzie et al., 1974; McKenzie and Weiss, 1975; Richter and Parsons, 1975) some form of flow in the mantle with a length scale of 700 km or less seems difficult to avoid, though as yet we have no observations about the form such flow takes. But if it occurs it must be driven by buoyancy forces which are not the direct result of plate production or destruction. Here we will assume that the only effect of the small scale on the large occurs through the mean temperature gradient. The small-scale flow must maintain a temperature gradient close to the adiabatic in most parts of the mantle and hence a reasonable approximation is to ignore all buoyancy effects outside the plates when considering the energetics of the large-scale flow. This approximation enormously simplifies the discussion because the equations governing the flow of material beneath the plates no longer explicitly involve the convection of heat. Whether such an approximation is justified is uncertain. Both scales of convection are strongly non-linear and can interact, but until more knowledge is forthcoming from laboratory or numerical experiments it seems sensible to ignore such possible complications.

Perhaps a more important difficulty is the probable existence of large-scale vertical motions unrelated to that associated with ridges and trenches. That such flows exist is strongly suggested by the long wavelength gravity anomalies determined from satellite motions. Many major anomalies are not obviously related to any present day plate boundaries, and the implied mantle flow may well be partly responsible for maintaining plate motions (see Section 5).

We will assume that the deformation of mantle materials can be described by a Newtonian viscosity, and allow the viscosity to be only a function of position. The equations are then linear and easily solved numerically. Such an approach is still basically kinematic, since the mantle motions are driven by motions of the boundaries. It does, however, allow a discussion of the forces which resist plate motion in terms of a possible fluid mechanical model, and in this respect is superior to the models used by Forsyth and Uyeda (1975) and by Chapple and Tullis (1977). They attempted to use the observed plate motions to determine the force balance on the major plates but did not explicitly consider the fluid dynamical forces resulting from the surface motions.

A most important feature of our model is that the motions are confined to the upper 700 km of the earth's mantle. Recently various authors (O'Connell, 1977; Davies, 1977a and b) have argued that convection associated with plate motions extends throughout the mantle. However, they have not put forward a

detailed model to account for the focal mechanisms within sinking slabs (Fig. 11). The state of stress indicated by the focal mechanisms is most easily explained by the inability of the slabs to penetrate deeper than 700 km. The observed mechanisms have always been and still are most difficult to account for by convection throughout the mantle, and none of the authors who favor such a flow have done so. No corresponding difficulty arises with the model used here.

In Section 4 the model is required to satisfy four observational constraints that are not in dispute. Three of these provide upper limits and one provides a lower limit on the mantle viscosity. These limits do not overlap for models having uniform viscosity, but it appears possible to construct a self-consistent model in which the mantle viscosity increases with depth.

## 2. The Model

In the absence of buoyancy forces the equations governing the motion of an incompressible fluid may be written:

$$\eta \nabla^2 \mathbf{u} = -\rho \nabla U + \nabla p \tag{1}$$

$$\nabla \cdot \mathbf{u} = 0 \tag{2}$$

where $\eta$ is the viscosity, $\rho$ the density, $\mathbf{u}$ the fluid velocity, $U$ the gravitational potential and $p$ the pressure. Both the density and the viscosity ate taken to be constant. If the flow is two-dimensional in the $x$, $z$ plane, $\mathbf{u}$ can be written in terms of a stream function

$$\mathbf{u} = \left( \frac{\partial \psi}{\partial z}, 0, -\frac{\partial \psi}{\partial x} \right) \tag{3}$$

and the curl of (1) becomes

$$\nabla^4 \psi = 0. \tag{4}$$

It is convenient to rewrite (4) as

$$\nabla^2 \zeta = 0 \tag{5}$$

$$\nabla^2 \psi = \zeta \tag{6}$$

where $\zeta$ is the vorticity, because fast subroutines are available for solving Poisson's and Laplace's equations. Though conversion of (1) and (2) into (5) and (6) is a convenient method of solving Stokes flow problems, it somewhat obscures the nature of the driving force. (1) shows that the flow is driven by the difference between the gravitational and pressure forces. In many fluid mechanical problems it is not necessary to determine the pressure, and a solution to (5) and (6) is sufficient. This is not the case here because we need to know the work done by rigid boundaries moving into the fluid. In the absence of flow (1) reduces to

$$\rho \nabla U_0 = \nabla p_0 \tag{7}$$

where $U_0$ and $p_0$ are the hydrostatic values for the gravitational potential and the pressure. When $\mathbf{u} \neq 0$

$$\begin{aligned} U &= U_0 + U_1 \\ p &= p_0 + p_1 \end{aligned} \tag{8}$$

and (1) becomes

$$\eta \nabla^2 \mathbf{u} = -\rho \nabla U_1 + \nabla p_1 \tag{9}$$

The term $-\rho \nabla U_1$ describes the influence of the gravity perturbation resulting from the flow on the fluid motions themselves, and is somewhat complicated to evaluate. Provided $\rho \nabla U_1 \ll \nabla p_1$ we may neglect the contribution of $\rho \nabla U_1$ to $\mathbf{u}$, even though we later need to obtain $\nabla U_1$ for comparison with the observations. The resulting error may be estimated from the expressions obtained by McKenzie (1968, Appendix D) and by Pekeris (1935) for the surface deformation and gravity field produced by low Rayleigh number thermal convection in a uniform viscous sphere. These expressions show that, when the wavelength of the circulation is $10^4$ km, the gravity anomaly is underestimated by about 30%, if $\rho \nabla U_1$ is neglected in (9), and the surface deformation by about 10%, decreasing to 15% and 5%, respectively, when the wavelength is 4000 km. Since we are only concerned with the order of magnitude of these two quantities, we may therefore neglect $\rho \nabla U_1$ in (9), which may be then written as

$$\eta \left( \frac{\partial \zeta}{\partial z}, 0, -\frac{\partial \zeta}{\partial x} \right) = \left( \frac{\partial p_1}{\partial x}, 0, \frac{\partial p_1}{\partial z} \right) \tag{10}$$

and hence $p_1$ is easily obtained. Since only $\nabla p_1$ enters (9), any arbitrary constant may be added to $p_1$. This indeterminancy allows us to choose an arbitrary origin for $p_1$.

In all cases we will consider, the motion will be driven by a rigid plate of thickness $t$ moving with a velocity $V$ and the layer in which the motion is occurring will have a depth $d$ (Fig. 1). It is therefore convenient to write

$$\begin{aligned} &\mathbf{u} = V\mathbf{u}', \quad \zeta = \frac{V}{d}\zeta', \quad x = dx' \\ &p_1 = \frac{\eta V}{d} p_1', \quad \psi = V d \psi', \quad z = dz' \\ &F = -\int p_1 \, dx, \; = -\eta V \int p_1' \, dx' \end{aligned} \tag{11}$$

where the primed quantities are dimensionless, and $F$ is the force/unit length. (10) then reduces to

$$\left( \frac{\partial \zeta'}{\partial z'}, 0, -\frac{\partial \zeta'}{\partial x'} \right) = \left( \frac{\partial p_1'}{\partial x'}, 0, \frac{\partial p_1'}{dz'} \right) \tag{12}$$

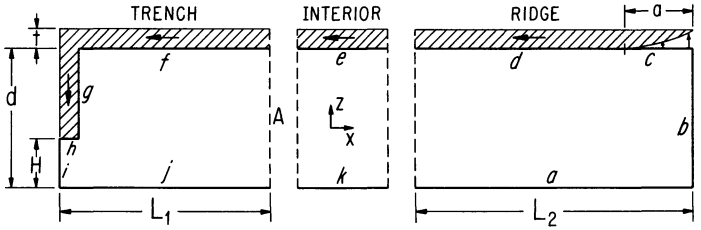


**Fig. 1.** Typical model for the large-scale flow, driven by dimensionless velocities imposed on the boundaries. Both components of the velocity vanish on *a*, *j*, and *k*. The normal component vanishes, but the tangential component is set to $-1$ on *d*, *e*, *f*, and *g*. On *b* and *i* the normal component of the velocity and the tangential stress vanish. On *h* the tangential velocity is zero and the normal component is $-1$. On *c* the normal velocity is given by (20). This model imposes reflection symmetry across both left and right hand edges, and was used to calculate the forces in Figures 4–6, and 8. Those in Figure 7 were obtained from a model with a more realistic boundary condition on the left

It is clear from the dimensionless forms of (5) and (6) that the solutions do not depend on $V$. Similarly the dimensionless values of the forces/unit length are independent of $V$, and the true forces $F$ can be obtained simply by multiplying by $\eta V$. This simplicity and generality is a consequence of the neglect of buoyancy forces in the fluid, and the assumption that $\eta$ is constant.

It is convenient to divide the circulation into three regions shown in Figure 1: The trench, the interior, and the ridge. This division resembles that made by Schubert and Turcotte (1972), who were concerned with the flow in the interior region. Sufficiently far from both ridge and trench regions, the stream lines must be horizontal and expressions for $\psi'$, $\zeta'$, and $dp_1'/dx'$ may be obtained analytically

$$\begin{aligned} \psi' &= (3t'+1)z'^2 - (2t'+1)z'^3 \\ \zeta' &= 2\{(3t'+1) - 3(2t'+1)z'\} \\ \frac{\partial p_1'}{\partial x'} &= -6(2t'+1) \end{aligned} \tag{13}$$

where $t' = t/d$ is the dimensionless plate thickness, the surface velocity is unity, and the total mass flux across any vertical plane is zero. The principal test we use to discover how far we need to be from the ridge and trench regions before (13) applies depends on the independence of $dp_1'/dx'$ on $z'$ in the interior. The interior solution for $\psi'$ is imposed as a boundary condition on the dashed line of either the ridge or the trench region (Fig. 1). For $\zeta'$ and $p'$ given by (13) to apply on the boundary, $dp_1'/dx'$ and hence $p_1'$, must be found to be independent of $z'$. Various cases are given in Figure 4, and show that the greatest variation of $p_1'$ with depth is less than 1 %.

We will also need the corresponding expressions when the shear stress vanishes on the upper surface of the viscous layer;

$$\psi' = \frac{t'}{2}(3z'^2 - z'^3)$$
$$\zeta' = 3t'(1-z') \tag{14}$$
$$\frac{dp_1'}{dx'} = -3t' \quad \text{(see also Appendix).}$$

Since the lateral extent of large plates is much greater than their thickness, the horizontal variation in $p_1'$ cannot be maintained by elastic forces within the plate but must be compensated isostatically. Therefore the appropriate boundary condition to apply at the surface is that the normal stress vanishes, and that $dp_1'/dx'$ is maintained by a surface slope $de'/dx'$ where $e'd$ is the change in elevation above a level surface due to the flow.

$$\frac{de}{dx} = \frac{1}{(\rho_m - \rho_w)g}\frac{dp_1}{dx} = \frac{\eta V}{(\rho_m - \rho_w)d^2 g}\frac{dp_1'}{dx'} \tag{15}$$

where $\rho_m$ is the density of the mantle, $\rho_w$ that of sea water. The gradient of the gravity anomaly corresponding to the surface slope is

$$\frac{d\Delta g}{dx} \approx 0.42\frac{\eta V}{g d^2}\frac{dp_1'}{dx'} \tag{16}$$

when $\Delta g$ is measured in $\text{mms}^{-2}$. Since $\rho$ is affected by the thermal structure of the plate, whereas the long wavelength components of $\Delta g$ are not, (16) is generally a more useful result than (15). This argument assumes that the lower boundary of the convecting region near 700 km is not deformed by the horizontal variation in $p_1'$. If deformation is possible (15) remains unchanged but the long wavelength components of the gravity field are removed by compensation (McKenzie, 1977). Under these conditions (15) is more useful. An additional complication occurs if the lower boundary results from a phase change. It may then be shown (McKenzie, in preparation) that (16) underestimates the size of $d\Delta g/dx$. Since it is not yet clear what is the nature of the boundary at a depth of 700 km, we use both (15) and (16) to estimate $\eta$.

The interior flow produces a viscous stress on the base of the plate, and the surface tilting causes a sliding force to act in the same direction. Both these forces therefore oppose the motion. The first of these gives a force/unit length

$$f_V = \frac{\eta V}{d}\zeta'\Big|_{z'=1} \tag{17}$$

whereas the sliding force/unit length $f_s$

$$f_s = -\frac{\eta V}{d}t'\frac{dp_1'}{dx'} \tag{18}$$

In the trench region the boundary conditions used are indicated in the captions to Figures 1 and 2. In some models a velocity of $-2$ was used on $g$ to discover whether a rapidly sinking slab could drag the surface plate towards the

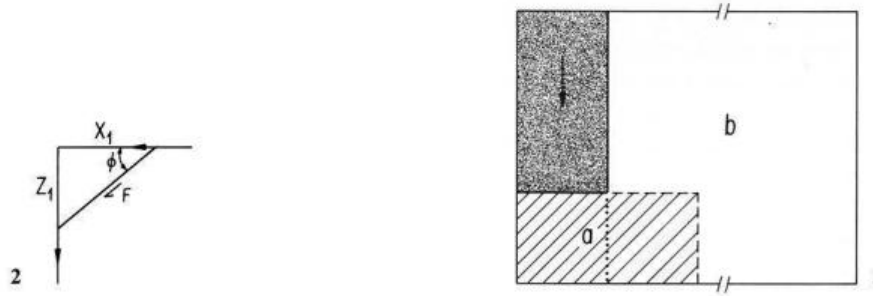


**Fig. 2.** The corner region at the trench. Because the velocity gradient is singular at the corner the stress is infinite. This region was excluded from the force balance calculations by neglecting the forces on $x_1$ and $z_1$, where $x_1 = 0.125$, $z_1 = 0.185$. The force $F$ on the oblique boundary was obtained from both the finite difference calculation and from a (singular) similarity solution

**Fig. 3.** Sketch to illustrate how the biharmonic equation was solved in the region beneath the slab tip. The equation was first solved in $b$ with $\psi' = \zeta' = 0$ on the dotted boundary, then this solution used to provide boundary conditions on the dashed boundary of $a$, and the process repeated by $b$. This iterative method converged rapidly

trench. The least realistic of the boundary conditions is that imposed on $i$. This boundary is only stress free if the flow has reflection symmetry about the left edge of the figure, and clearly this is a poor approxiamtion: Real trenches are strongly asymmetric. We therefore also carried out calculations on a more realistic asymmetric model.

The basic numerical method used to solve (5) and (6) in the presence of rigid boundaries was described by Richter (1973a). All the calculations described below used 32 vertical mesh points and square elements. However, certain difficulties arise in applying finite difference shemes to the trench region. Because the position of the boundary $A$ in Figure 1 is arbitrary, the value of $L_1$ should not affect the solution. If, however, (13) is imposed as a boundary condition on $A$ and $L_1$ is small, the flow will be strongly affected by the value chosen, whereas if $L_1$ is made large, computer time will be wasted since a large part of the solution will be indistinguishable from (13). It is undesirable to increase the mesh spacing since in places the vorticity varies rapidly. A convenient test was the constancy of $p_1'$ on $A$. Since the pressure in the interior flow should only be a function of $x'$, too small a value of $L_1$ produced some variation with $z'$. This and other simple tests showed that a value of 1.5 was a good compromise.

The most obvious objection to the boundary conditions imposed in Figure 1 in the trench region is that they require a singularity in the vorticity in the upper left hand corner. The singularity occurs because the velocity is not continuous, and it is not obvious that the numerical scheme will model this region accurately. Furthermore, the similarity solution for the flow in this corner (Hewitt et al., 1975) shows that the shear forces acting on the horizontal and vertical boundaries are infinite. The mathematical cause of this singularity is that the velocity is not continuous and hence the stress, which depends on the gradient of the velocity, is infinite. Such singularities commonly arise in fluid mechanics

when the equations used to describe the physical behavior of the system locally no longer do so. In this example the relationship between stress and strain rate ceases to be linear when the stress exceeds a particular value. Unless solutions to the non-linear equations are obtained we must exclude the corner region from the calculations of force balance. We did this by cutting off the region with an oblique surface at an angle $\phi$ to the horizontal (Fig. 2). and calculating the force $F'$ which the flow exerted on this surface. When $\phi = \pi/4$, the value of $F'$ is easily obtained from the similarity solution:

$$F' = 2\sqrt{2} \Big/ \left(1 + \frac{\pi}{2}\right) \doteqdot 1.10 \tag{19}$$

It must be independent of the position of the surface because there are no length scales in the similarity solution. The corresponding value from the numerical solution was 1.07 when the surface intersected 4 grid points from the corner. Such good agreement is somewhat surprising, and shows that the singularity in the vorticity does not produce undesirable numerical effects.

The last difficulty in the trench region results from the geometry of the fluid. The numerical schemes we used can only solve the equations in rectangular regions. We overcame this problem by using two overlapping regions shown in Figure 3, and iterating between the two. The first step consisted in solving for $\psi'$ and $\zeta'$ in region $b$ with $\zeta' = \psi' = 0$ on the dotted part of the boundary. The resulting solution was then used as a boundary condition on the dashed part of the boundary of region $a$. This solution was in turn used for boundary conditions for region $b$. Ten such iterations were used, and the maximum difference in $\psi'$ in the overlapping region was 1 part in $10^4$. The accuracy of this numerical procedure was tested by carrying out a simple experiment, described in detail elsewhere (Richter, 1977). A buoyant rectangular rod was allowed to rise through a layer of glycerine. Since the buoyancy force depends only on the cross sectional area of the rod and the density contrast between the rod and the glycerine, the driving force is known. The calculated and observed velocities showed excellent agreement, and therefore confirm the accuracy of the iterative scheme.

The ridge region contains no features not present in the trench region. A simpler model would not possess the boundary $c$, and $d$ would continue to meet $b$. However, such a model would possess a vorticity singularity and would also have no boundary where material could flow out of the region. Both difficulties may be avoided by introducing a free boundary $c$ of width $a = da'$ on which the normal velocity is specified:

$$U_z' = \frac{2t'}{a'^2}(x' - L_2 + a'). \tag{20}$$

Such a boundary seems reasonable beneath a ridge, where the partial melting and the elevated temperature are likely to decouple the surface plate motions from those of the mantle below. Since $d$ is a rigid boundary and $c$ is not, there is a discontinuity in vorticity where they meet. The same arguments as before apply to the choice of $L_2$, which was taken to be 2.

Though the model outlined above is obviously an approximation to the full mantle circulation problem it is nonetheless a self-consistent convective model (except in the corner region near the trench where the singularity is present). Hence within the limitations of our model we take full account of all fluid dynamical forces. The unusual form which some of these forces take arises because of mass transfer across boundaries $h$ and $c$ in Figure 1 and the work done by other moving boundaries. It is important to emphasize that these forces are not artifacts of our particular model and that exactly the same forces are found in a continuously deforming material if one isolates particular parts of the system.

## 3. Forces

*Resistive Forces*

The results of the calculations using the model in Figure 1 are shown in Figures 4–8. The ridge models in Figure 4 have a variable width of boundary on which the vertical velocity is non-zero and given by (20). Since the plate thickness is small compared to the thickness of the layer, flow which is driven by the mass flux across the boundary is weak compared with that driven by the

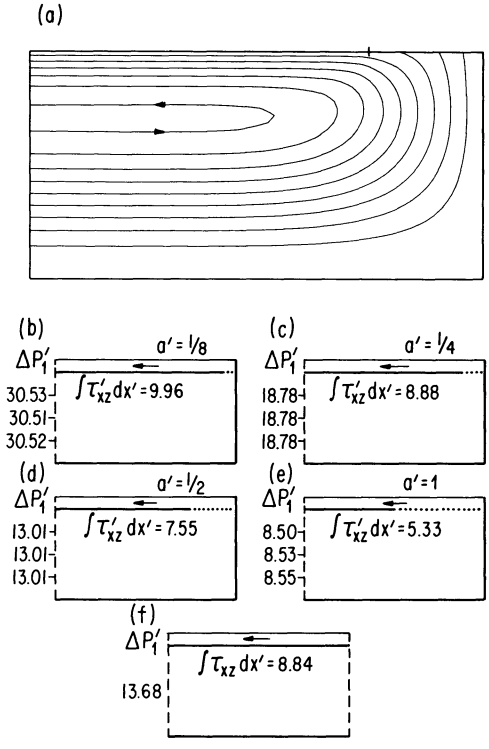


**Fig. 4a–f.** Ridge models with a plate moving to the left with $u'_x = -1$ for various values of $a'$. The width of the region is twice the depth. $\int \tau'_{xz}\, dx'$ is the dimensionless force/unit width which resists the motion of the plate. $\Delta p'_1$ is the dimensionless pressure difference between points at depths of $\frac{1}{4}$, $\frac{1}{2}$, and $\frac{3}{4}$, and the ridge axis at the top right. **(f)** shows the resistive force and pressure drop of the corresponding interior solution. The vertical velocity imposed on the dotted boundary is given by (20). The contour interval for $\psi'$ in (a) is 0.022 and $t' = 4.5/32$

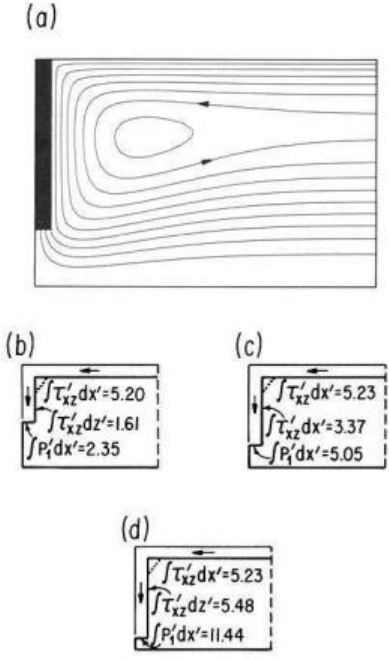


**Fig. 5a–d.** Trench models, symmetric about the left hand boundary, with a sinking slab moving vertically with $u'_z = -1$ and the plate moving horizontally with $u'_x = -1$. The region extends a distance of 1.5. The mass flux through the tip of the slab and through the right hand boundary is $Vt/2$. $\int \tau'_{xz}\, dx'$ is the force/unit width resisting the plate motion, excluding the part to the left of the dotted line within 9/64 of the corner singularity. $\int \tau'_{xz}\, dz'$ is the force/unit width acting on one side of the sinking slab, excluding the part above the dotted line. $\int p'_1\, dx'$ is the force/unit width due to the pressure difference between the right hand edge of the region and the tip of the slab. The force/unit width acting on the dotted line is 1.10 and is a driving, not a resistive, force. It is not included in the force balance calculations. The contour intervals for stream lines in (1) is 0.022, and the slab extends to a depth of $\frac{1}{2}$ in (**b**), $\frac{3}{4}$ in (**c**), and $\frac{7}{8}$ in (**d**)

horizontal plate motion. Hence the major upwelling does not occur beneath the ridge axis but where the boundary condition changes to fixed horizontal velocity. The various models for a ridge in Figure 4 should be compared with the corresponding interior solution (Fig. 4f). Only those models with a total width of prescribed upwelling smaller than $\frac{1}{4}$ have significantly greater resistive forces than those of the corresponding interior solution. There is at present no information about the half width of the region below the ridge axis where the viscosity is strongly reduced. It is not even known whether this region is limited to the ridge axis or extends beneath all plates and decouples their motion from that of the mantle below (see section 4). This ignorance suggests that it is at present unnecessary to use anything more sophisticated than the interior solution when calculating the resistive forces near ridges.

The forces near trenches are considerably more complicated. The simplest model consists of a slab sinking vertically with velocity $-1$ (Fig. 5). The resistive force $\int \tau'_{xz}\, dx'$ which acts on the horizontal plate is infinite if evaluated from the point in contact with the sinking slab. As explained in the last section, this corner region was excluded from the calculations (Fig. 2). The remaining force is slightly less than the corresponding interior solution for a plate of width 1.5. The force acting on the dotted line in Figure 5 is a driving force of small magnitude (1.10). It was not included in the force balances because it is not a true source of work, but results from the exclusion of the singularity. The force acting on the side of the sinking slab $\int \tau'_{zx}\, dz'$ also is infinite if integrated from the corner, but once again this region is excluded. Since large velocity gradients occur when the

tip of the sinking slab approaches the lower boundary of the layer, the magnitude of this force depends strongly on the length of the sinking slab.

The most important force $F'_p$ acts on the tip of the sinking slab and involves the perturbed pressure $p'_1$.

$$F'_p = \int_0^{t'} p'_1 \, dx'$$

The origin of $p'_1$ was chosen to be the ridge axis. It is convenient to divide $p'_1$ into three contributions: the first due to the flow in Figure 4, the second due to the interior flow and the third due to the flow near the trench. Only the third contribution is shown in Figure 5. If the plate width is greater than 1.5, a term due to the interior flow must be added. $F'_p$ represents the work that must be done to transfer mass from the tip of the slab to the ridge axis. It is not present if the slab and plate have no thickness. It is clear from the numbers in Figure 5 that, even without the contribution from the interior, $F'_p$ is greater than the shear force on the vertical boundary of the sinking slab. Within a convecting fluid the same result holds: the pressure considerably exceeds the shear stress (McKenzie, 1977). This result is only apparent if $p'_1$ is calculated, which it rarely is.

Besides the fluid dynamical forces acting on the bases and edges of plates, forces act on the faults which form plate boundaries. These forces can be divided into two components, one in the plane of the fault and one normal to it. The first component is involved in the generation of earthquakes, and most of the information about its magnitude has been obtained from detailed investigations of the radiated seismic waves. Studies of a number of large earthquakes (Kanamori, 1970a, 1971; Wu and Kanamori, 1973; Fukao, 1973) have shown that the difference between the initial and final stress is between $2 \times 10^6$ and $5 \times 10^6$ newtons $m^{-2}$. There is at present no evidence that either the stress or the stress drop depend on the type of plate boundary involved. On ridges the earthquakes produced by motion on both normal and strike slip faults are shallower than 10 km (Weidner and Aki, 1973; Prothero et al., 1976). Also on rapidly spreading ridges, with plate separation rates of 60 mm $yr^{-1}$ or more, earthquakes are rare and small, and large normal faults are also absent. We will therefore ignore frictional resistance between separating plates.

The importance of transform faults is less clear. They are generally almost vertical, and those that have been studied in detail release little seismic energy below 12 km. If the resistive forces were zero below this depth their contribution to the force balance could be ignored. Since, however, plates are more than 80 km thick the absence of earthquakes is unlikely to result from the absence of stresses, but is more likely to be due to a change in the behaviour of deforming rocks. If the stress on transform faults is $10^7$ newtons $m^{-2}$ and extends to a depth of 100 km it could strongly influence plate motions. Chapple and Tullis (1977) included a resistive force due to transform faults in their analysis of the forces controlling plate motions, but found that its magnitude was too small to be determined. We chose to ignore this contribution to the plate motions principally because it can only be introduced into a two-dimensional force balance model in an arbitrary way.

In contrast to the forces from ridges and transform faults, those acting on the thrusts beneath island arcs are probably an order of magnitude greater because the dip on the faults is small. If a shear stress $\sigma$ acts on the fault whose dip is $\theta$, the resulting horizontal force $F$ on the plate of thickness $t$ is $\sigma t/\tan\theta$ in a direction normal to the strike of the fault. Taking $t=85$ km and $\sigma=10^7$ newtons $m^{-2}$ gives $F=4.8\times10^{12}$ newtons $m^{-1}$ when $\theta=10°$ and $F=2.3\times10^{12}$ newtons $m^{-1}$ when $\theta=20°$. The magnitude of this force is independent of the plate velocity and should be included in any force balance. This is easily done because the density variations near ridges produce a driving force $F_R$ of $2\times10^{12}$ newtons $m^{-1}$ (see below) which balances the resistive force at trenches within the uncertainty of both calculations. Hence neither need be explicitly included. This convenient equality may, however, conceal the importance of these forces, since both are large compared with those in the two layer model considered in section 4, and the uncertainty in the value of $F-F_R$ is large. Since $F_R$ acts near ridges and $F$ on the thrust plane beneath island arcs together they keep plates in compression. For the same reason plates surrounded by ridges must also be in compression. Such a stress state agrees with the limited observations available concerning the stress state within plates (Sbar and Sykes, 1973; Rayleigh et al., 1972).

No information about the normal component of the force acting on faults can be obtained from earthquakes, and nothing is yet known about its magnitude and importance, or even whether this component acts as a driving or resistive force. Despite this ignorance there is some evidence (see Molnar and Tapponnier, 1975) that normal forces acting in some continental regions do control the motion of some large plates. Despite this evidence we chose to ignore such forces everywhere, partly because their magnitude is unknown, and partly because their importance depends on the shape of individual plates.

In Figure 5 the plate and the slab move with the same velocity. This is a sensible model to use if the slab and plate are connected and stress can be transmitted from one to the other. However, recent work on earthquakes produced by normal faulting within the plate and slab strongly suggests that the faults extend through the plate (see McKenzie and Weiss, 1975). If all plates are broken in this way, any stress transmission that occurs must do so either by frictional forces within the plate and slab or by viscous forces acting on their boundaries. In the absence of the sinking slab the resistive force on the plate of length 1.5 would be 6.63 (Fig. 4f) and it is clear from Figure 5 that a slab sinking with velocity $-1$ has little effect on this force. If viscous forces are to transmit the force, the slab must sink faster than $-1$. Since the mass flux is fixed, the slab can only sink faster if its thickness is less than $t$. Figure 6 shows the forces acting when the slab sinks at $-2$ and is half the thickness of the surface plate. The force resisting the plate motion is reduced but it not negative, even though the width of the plate in Figure 6 is only 1000 km. Clearly considerably larger sinking velocities are needed if plates the size of the Pacific are to be moved by viscous forces. Because mass must be conserved, larger velocities require thinner slabs, and it is not obvious how a plate can become a thin rapidly moving slab at shallow depths beneath a trench.

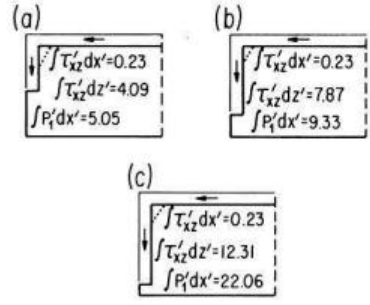


**Fig. 6a c.** As for Figure 5 but with the slab sinking with $u'_z = -2$. The driving force/unit width on the dotted line is 1.36 and is omitted in the force balance calculations. The mass flux through the tip of the slab and the right hand boundary is $Vt$

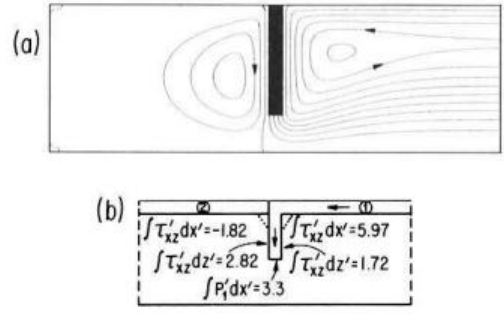


**Fig. 7a d.** Model for an asymmetric trench with the slab sinking with $u'_z = -1$, plate 1 moving to the left with velocity $-1$ and plate 2 stationary. The integrals are taken over the same boundaries as in Figure 5. The forces on the base of plate 2 act to the right. The mass flux through the right hand boundary is $Vt$, that through the left hand zero. The contour intervals for $\psi'$ in **(a)** are 0.02866, the slab extends to a depth of $\frac{1}{2}$ in **(b)**, $\frac{3}{4}$ in **(c)** and $\frac{7}{8}$ in **(d)**. The perturbed pressure on the right hand boundary is taken to be zero

### *Driving Forces*

Since the oceanic crust is produced by partial melting of the mantle, large scale differences in density can only be produced by differences in temperature. Hence all the driving forces are convective in origin. Horizontal temperature variations beneath ridges produce both the shallow bathymetry and a driving force $F_R$, whose magnitude may be obtained from any thermal model of a spreading ridge. A simple model consists of isothermal hot material of density $\rho_m$ upwelling at the ridge axis, then cooling as it moves away until the temperature gradient is constant across the plate of thickness $t$. The density at the base of the plate is everywhere $\rho_m$. If the elevation difference between the ridge axis and the

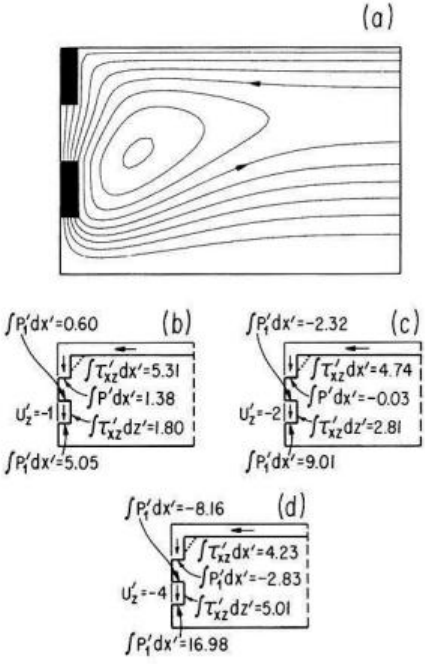


**Fig. 8a–d.** As for Figure 5, but with a piece of slab detached, and sinking with various different velocities. The contour interval for $\psi'$ in (**a**) is 0.0308, and the flow corresponds to (**c**). A negative pressure integral corresponds to a resistive force on the upper boundary of the sinking block. The length of both the slab and the block is $\frac{1}{4}$

cooled plate is $e$, the density of sea water is $\rho_w$, then the pressure $P_1$ beneath the ridge axis at a distance $z$ above the base of the plate is

$$P_1 = (\rho_m - \rho_w)\, g(t + e - z) \tag{21}$$

When the plate has cooled and a linear temperature gradient has become established between the mantle and the sea floor, the density within the plate $\rho_p$ increases linearly with $z$:

$$\rho_p = \rho_m - \rho_w + \beta z \tag{22}$$

where $\beta$ depends on the thermal expansion coefficient. Integration gives $P_2$, the pressure beneath old sea floor

$$P_2 = g(\rho_m - \rho_w)(t - z) + \frac{g\beta}{2}(t^2 - z^2). \tag{23}$$

Since the ridge is taken to be in hydrostatic equilibrium $P_1 = P_2$ when $z = 0$. Thus

$$\beta = 2(\rho_m - \rho_w)\, e/t^2. \tag{24}$$

We can now obtain the driving force due to ridge pushing by integration

$$F_R = \int_0^{t+e} P_1\,dz - \int_0^{t} P_2\,dz = g\,e(\rho_m - \rho_w)\left(\frac{t}{3}+\frac{e}{2}\right). \tag{25}$$

Only a small part of this force arises from the tendency of the plate to slide down the sides of the ridge. If the uplift of the upper surface is prevented by applying normal forces, the pressure still exerts a force $F_2$ where

$$F_2 = \int_0^{t} P_1\,dz - \int_0^{t} P_2\,dz = g\,e(\rho_m - \rho_w)\frac{t}{3}. \tag{26}$$

$F_2$ originates from ridge pushing and $F_R - F_2$ from plate sliding. Substitution from table 1 gives $F_R = 2\times10^{12}\ \mathrm{nm}^{-1}$ and $F_R - F_2 = 10^{11}\ \mathrm{nm}^{-1}$, and therefore most of the force is due to ridge pushing. The estimate of $F_R$ is probably accurate to within a factor of 2, and corresponds to a shear stress of $1.2\times10^{7}\ \mathrm{nm}^{-2}$. Except in rare cases oceanic plates do not fail under this stress, which therefore places a lower limit on the shear strength of the oceanic lithosphere.

**Table 1**

| | | | |
|---|---|---|---|
| $t$ | $=85\ \mathrm{km}$ | $T_1$ | $=1200°\mathrm{C}$ |
| $e$ | $=3\ \mathrm{km}$ | $\alpha$ | $=3\times10^{-5}\,°\mathrm{C}^{-1}$ |
| $\rho_m$ | $=3.3\ \mathrm{Mg\,m}^{-3}$ | $C_p$ | $=1.2\times10^{3}\ \mathrm{J\,kg}^{-1}\,°\mathrm{C}^{-1}$ |
| $\rho_w$ | $=1.0\ \mathrm{Mg\,m}^{-3}$ | $k$ | $=3.1\ \mathrm{W\,m}^{-2}\,°\mathrm{C}^{-1}$ |
| $g$ | $=9.8\ \mathrm{m\,s}^{-2}$ | $d$ | $=615\ \mathrm{km}$ |

The other source of convective energy results from density contrasts associated with trenches. The most important is undoubtedly the density contrast between the sinking slab and the surrounding mantle, and its magnitude may be estimated from the thermal structure (McKenzie, 1969).

$$F_t(z) = \frac{8\,g\,\alpha\,\rho_m\,T_1\,t^2}{\pi^4} R\left\{\exp\left(-\frac{\pi^2}{2R}\frac{z}{t}\right) - \exp\left(-\frac{\pi}{2R}\frac{d}{t}\right)\right\} \tag{27}$$

where

$$R = \frac{\rho_m\,C_p\,V\,t}{2\,k} \tag{28}$$

$\alpha$ is the coefficient of thermal expansion, $T_1$ the temperature difference between the bottom of the ocean and the mantle, $z$ the depth below the base of the plate, $k$ the thermal conductivity and $C_p$ the specific heat. Substitution gives $R = 1.7\,V$ where $V$ is in mm yr$^{-1}$. Assuming that the slab sinks vertically, the total driving force $F_t(0)$ is plotted as a function of $V$ in Figure 9. When $V$ is small

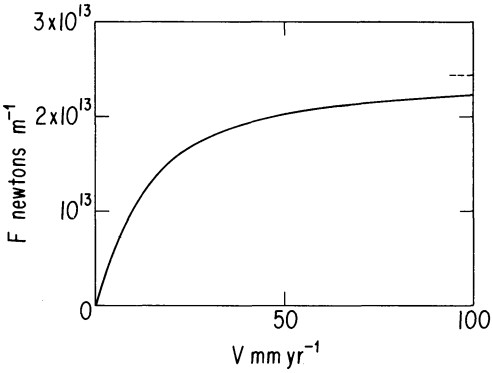


**Fig. 9.** Available driving force from subducted slab as a function of the consumption velocity $V$, obtained from (27). The horizontal dashed line shows the asymptotic limit as $V \to \infty$

($\lesssim 10$ mm yr$^{-1}$) the last term in (27) may be neglected, and $F_t(0)$ increases linearly with $V$. Under such conditions the temperature of the slab's interior has become approximately $T_1$ when it reaches the base of the upper mantle. If, however, $V$ is large then (27) may be written

$$F_t = \frac{4 g \alpha \rho_m T_1 t}{2} (d - z) \tag{29}$$

and is independent of $V$. The expression is appropriate when $V \gtrsim 40$ mm yr$^{-1}$ and the slab sinks with little increase in temperature. Figure 9 shows the maximum force available from a sinking slab. When the slab reaches the base of the upper mantle at a depth of 700 km, we are assuming that the cold material must flow horizontally and does not contribute to $F_t$. The force actually exerted will be less because the slab does not remain intact as it descends, but breaks up into blocks. The motion between these blocks produces intermediate and deep focus earthquakes. Studies of the stress involved in such shocks (Wyss, 1970; Wyss and Molnar, 1972; Fukao, 1972; Mikumo, 1972) have found some evidence that intermediate shocks may involve somewhat larger stress drops than either shallow or deep earthquakes. However, we are only concerned with the force which can be transmitted to the plates, and hence with the stress within the shallow part of the slab beneath the front of the island arc. We will therefore impose an upper limit of $2 \times 10^7$ newtons m$^{-2}$ on the stress within this part of the slab. In the absence of resistive forces it is clear from Figure 9 that this stress will be exceeded in slabs sinking faster than about 3 mm yr$^{-1}$. The consumption rate in all major trench systems is greater than this limit, and therefore failure of the sinking slabs may occur. Whether or not it does so depends on how the buoyancy forces are balanced by resistive forces.

These two contributions to the driving forces are generally recognized and easily calculated. Two others are not. Probably the most important of these results from large-scale flow which is not driven by plate motions. At present the only evidence for the existence of such flow comes from long-wavelength gravity anomalies determined from satellite motions (Gaposchkin, 1974; Lerch et al., 1974). As explained above, flow associated with these anomalies may make a large contribution to the perturbed pressure field and the viscous

stresses. The other driving force which could help maintain the motions results from the topography of trenches. A driving force may arise in the same way as that at ridges. Because mantle rock is replaced by water the lithostatic pressure at all depths is reduced by $(\rho_m - \rho_w) g H$ where $H$ is the depth of the trench. However, unlike ridges, trenches are not isostatically compensated and must be maintained by elastic forces. Unfortunately, very little is yet known about the distribution of these stresses. It is not even clear whether any of the pressure reduction is available to drive the plates. Therefore this possible energy source or sink is also neglected.

## 4. Observational Constraints and Force Balance

*Gravity*

If the model discussed in section 2 is to provide a useful description of the large-scale flow it must be compatiable with relevant geophysical observations. Since the only major uncertainties are the value of the viscosity and its variation with depth we use the observational constraints to impose constraints on the viscosity.

The simplest constraint to apply depends on the absence of large long wavelength gravity anomalies. The gravity anomaly produced by the flow in Figure 1 is complicated and difficult to calculate near the ridge and trench regions where large horizontal density contrasts must exist and elastic forces are important. In the interior region, however, the gravity anomaly should increase linearly towards the trench, and is produced by the horizontal pressure gradient (see Eq. (16)). Hence we can impose a bound on the viscosity by considering the horizontal gradient of the gravity field across interior regions of plates remote from their boundaries. The long wavelength pressure gradient will "tilt" the sea floor because the plates are thin and flexible. The observed difference in gravity between trenches and ridges is less than about $0.3\ \text{mm s}^{-2}$ and is positive over trenches. Since the return flow should produce an anomaly which varies linearly between trenches and ridges, whereas the observed field consists of a positive anomaly centered on the trenches whose extent is only a fraction of that of the plate (Gaposchkin, 1974; Lerch et al., 1974), this value is probably an upper limit. To obtain the magnitude of the gravity anomaly from the expression in section 2 we need the horizontal extent and velocity of the plate. In the discussion below we will consider two plates. The first, plate $A$, moves at $100\ \text{mm yr}^{-1}$ and has a lateral extent of $10^4$ km. These values are comparable to those of the Pacific plate. The second, plate $B$, moves at $50\ \text{mm yr}^{-1}$ and has an extent 6000 km. These values resemble those for the Indian-Australian plate. If the viscosity of the mantle below the plates is constant, then the upper limit on the viscosity and stress on the base for the two plates is

$$\begin{aligned} &\eta_A \lesssim 10^{19}\ \text{kg s}^{-1}\,\text{m}^{-1}, && \sigma_A \lesssim 2.6 \times 10^5\ \text{newtons m}^{-2} \\ &\eta_B \lesssim 3.3 \times 10^{19}\ \text{kg s}^{-1}\,\text{m}^{-1}, && \sigma_B \lesssim 5.2 \times 10^5\ \text{newtons m}^{-2}. \end{aligned} \tag{30}$$

If, however, there is a thin layer of very low viscosity material beneath the plates (Appendix) then the horizontal pressure gradient required to drive the return flow is much reduced and the corresponding expressions are

$$\eta_A \lesssim 1.9 \times 10^{20}, \quad \eta_B \lesssim 6.4 \times 10^{20} (\mathrm{kg\,s^{-1}\,m^{-1}}) \tag{31}$$

from (14) and (16). The shear stress on the base of the plates is also greatly reduced in both cases.

There are several objections to using the gravity field from our simple model to obtain an upper limit on the allowable viscosity. The most obvious is that the sign of the gravity anomaly obtained in section 2 is opposite to that obtained by McKenzie et al. (1974). Since the model we use here contains no buoyancy forces within the fluid whereas the numerical models used by McKenzie et al. do, the disagreement in sign could be due to such forces. If this were the case no limits such as (30) and (31) could be obtained. Fortunately this is not true. Recent convective calculations by McKenzie (1977), using a temperature dependent viscosity, have shown that the sign of gravity anomaly over a rising region changes from positive to negative when the viscosity variation is sufficiently large. This change in sign results from a change in sign of the horizontal gradient of $p_1$. The model used here contains a plate at the surface, rather than a high viscosity region, but is otherwise similar to the convective models. There is therefore no reason to suppose that buoyancy forces and density variations in the mantle invalidate the limits (30) and (31).

The argument above depends on the mechanical behavior of the lower boundary of the convecting region. This question has been discussed above in section 2. If the lower boundary cannot be deformed vertically or is a phase change, then (31) applies. If, however, the lower boundary is deformable, then the long wavelength gravity anomalies are compensated (McKenzie, 1977) and only the elevation differences limit $\eta$. Unfortunately most of the variations in bathymetry are produced by variations in the temperature of the plates and thus a large and uncertain correction must be applied to obtain the dynamic variation produced by $dp_1/dx$ (Parsons and Sclater, 1977). Though the thermal models fit the observed variation of age with depth to within the observational errors, the models were constructed to do so. Since Parsons and Sclater could fit the observations from all major ocean basins with a single curve of depth as a function of age, it seems unlikely that the return flow can produce more than about 1 km variations in depth not associated with gravity anomalies. If this rather uncertain limit is used to obtain estimates of the viscosities from (15) we obtain

$$\begin{aligned} &\eta_A \lesssim 3.5 \times 10^{19}\ \mathrm{kg\,s^{-1}\,m^{-1}}, \quad \sigma_A \lesssim 8.7 \times 10^{5}\ \mathrm{nm^{-2}} \\ &\eta_B \lesssim 1.2 \times 10^{20}\ \mathrm{kg\,s^{-1}\,m^{-1}}, \quad \sigma_B \lesssim 1.5 \times 10^{6}\ \mathrm{nm^{-2}} \end{aligned} \tag{32}$$

if there is a single layer, and

$$\eta_A \lesssim 6.1 \times 10^{20}, \quad \eta_B \lesssim 2.1 \times 10^{21}\ \mathrm{kg\,s^{-1}\,m^{-1}} \tag{33}$$

if there is a low viscosity layer beneath the plates.

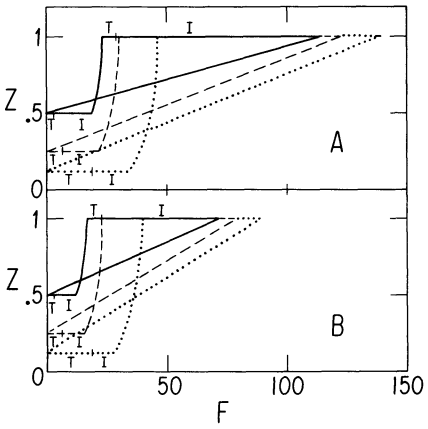


**Fig. 10 A and B.** Force balance diagrams for plate A, 10,000 km long (**A**), and plate B, 6000 km long (**B**) in units of $\eta V$, all for the asymmetric models in Figure 7 and constant viscosity. The vertical scale on the left shows the dimensionless depth to which the slab reaches beneath the trench. The horizontal line extending to the right from the tip shows the resistive force due to the local pressure field within a distance of 1.5 from the trench, marked *T*, and that due to the interior pressure, marked *I*. The curved line drawn from the tip of the slab to the surface indicates the shear force exerted on the sides of the sinking slab integrated upwards from their base. Their magnitude is correct but the depth dependence is sketched. The horizontal lines at $z'=0$ show the total horizontal resistive force acting on the base of the plates due to both the region near the trench and the interior. The interior force includes both $f_v$ and $f_s$ (Eqs. (17) and (18)). For the two cases where the tip extends to $z'=0.5$ these two contributions are marked *T* and *I*. The gravity force due to the slope of the surface has been included in *I*. The oblique straight lines show the integrated buoyancy and must close the diagrams. The reciprocal of their slopes correspond to the buoyancy force in units of $\eta V$ exerted by a constant density contrast between the sinking slab and the surrounding mantle which are necessary to maintain the plate motions. The slab will be subject to extensional stress at those depths where the integrated buoyancy is greater than the cummulative resistive force up to that depth. When the integrated buoyancy is less than the cummulative resistive forces, the slab will be in downdip compression. The continuous line shows the forces for $z'=0.5$, dashed for $z'=0.75$ and dotted for $z'=0.875$

## *Force Balances*

All other constraints we impose depend on the balance between resistive and driving forces, and are most easily understood using a force balance diagram (Fig. 10). Since forces due to the inertia of the mantle material are extremely small compared with the viscous forces, the forces driving the plate and slab must exactly balance the resistive forces. Figure 10 shows the cummulative resistive forces and the integrated driving force (buoyancy force) starting from the bottom of the downgoing slab. Since the total resistive and driving forces must be equal in magnitude, the two curves for each case must form a figure closing at $z'=1$. Furthermore, where the cummulative resistance exceeds the integrated buoyancy, (near the bottom of downgoing slab) the slab will be in compression. Where the opposite is true (nearer the surface) the slab is in tension. These terms are somewhat misleading. Since all principal stresses are everywhere negative the failure is always a shear failure. When the slab is in

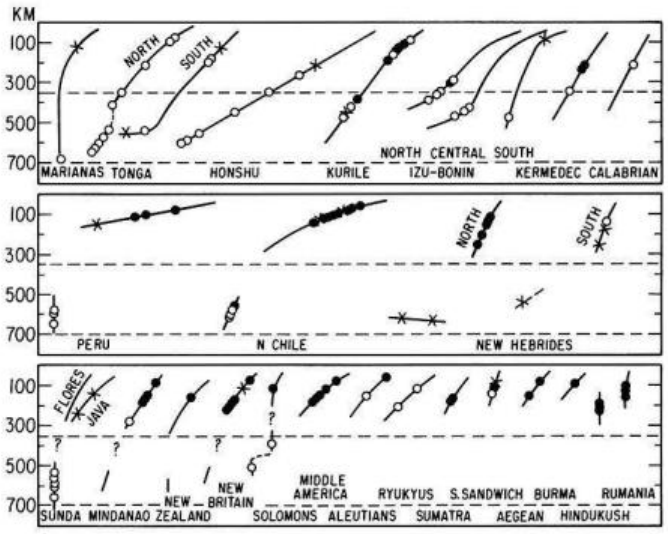


**Fig. 11.** Summary of the stress state within sinking slabs (Isacks and Molnar, 1971). Open (closed) circles represent zones where the $P(T)$ axis of the fault plane solutions is approximately coincident with the dip of the sinking slab, described as compression (tension). Crosses mark solutions which showed no simple relationship between the stress state and the slab geometry. Continuous curved lines represent the shape of the seismic zone. The upper horizontal dashed line at a depth of 350 km marks the approximate depth below which the slabs are in compression; no earthquakes have been recorded at a depth greater than that of the lower dashed line

tension shear failure permits it to lengthen, whereas when it is in compression it must shorten if a shear failure occurs. Most models of island arcs assume that the slabs move with the same velocity as that of the plate being consumed, despite the existence of intermediate and deep focus shocks. It is, however, hard to exclude major variations in velocity associated with slab deformation, and we have therefore considered models in which part or all of the sinking slab sinks with greater velocity.

The pressure forces acting on the slab tip consists of two parts. The first, marked $T$ in Figure 10, results from the local flow near the trench. The second, marked $I$, is due to the interior flow. Since the second contribution is independent of the depth to which the slab extends, and depends only on the distance between the trench and the ridge, the lower part of the slab must always be in compression. When the slab approaches the base of the layer the local contribution becomes very large and may exceed the buoyancy force of the entire slab. Under these conditions the plate will be in compression at all depths.

Fortunately it is possible to use fault plane solutions of earthquakes within the sinking slabs to discover whether they are in tension or compression. Figure 11, from Isacks and Molnar (1971), shows the extent and the stress state of most known slabs. It shows that slabs whose tips do not reach below a depth of 350 km are in tension throughout most of their length. Though few mechanisms are available from close to the tips of these slabs (Fig. 11), they must always be in compression. If the tip of the slab extends deeper than 350 km, but

less than 600 km, then the part above 350 km is in tension, that below in compression, whereas if the tip extends below 600 km the slab is in compression throughout is length. The force balance diagram must satisfy these constraints. The observations from the Kermadec and Kurile Arcs (Fig. 11) suggest that the lower 150 km of the slab are in compression. This value will be used for plate $A$, since the return flow from these two arcs must extend to great distances. Other arcs, such as Middle America where all the solutions are tensional, have correspondingly shorter return paths. Other arcs with slabs, such as those beneath the Aleutian and Ryukyu Islands, extending to a similar depth to that beneath Middle America have longer portions of the slab in compression, suggesting that the difference is not due to depth of penetration alone. One further condition we impose is that pieces of the slab should be able to fall through 600 km driven by their own buoyancy. In all but one case the existence of detached blocks gives little information because the consumption rate in the past is unknown. The sole exception is New Zealand, where the consumption rate is known from the magnetic anomalies on the Pacific-Antarctic and Southeast Indian Rises. The mean rate over the last 10 My is about 10% less than the present rate (Molnar et al., 1975). Beneath the North Island of New Zealand the sinking slab is continuous to a depth of about 300 km, then there is a gap, followed by a few shocks spread over 50 km at a depth of about 600 km (Fig. 11). It is only possible to form such a structure with little variation in consumption rate if small blocks can sink through the mantle below a depth of 300 km at velocities greater than the rate of 30 mm/yr at which the slab has been sinking (Christoffel and Calhaem, 1973).

*A One-Layer Mantle*

If the sinking slab extends to a depth of 630 km and the buoyancy forces (from Fig. 9) are balanced by viscous forces, then the viscosity can be obtained from the force balance diagrams in Figure 10. That for plate $A$ gives

$$\eta_A \simeq 5 \times 10^{19} \text{ kg s}^{-1} \text{ m}^{-1}$$

and plate $B$

$$\eta_B \simeq 1.6 \times 10^{20} \text{ kg s}^{-1} \text{ m}^{-1}$$

The mean stress $\sigma$ acting on the sides of the sinking slabs is

$$\sigma_A \simeq 2.8 \times 10^6 \text{ newtons m}^{-2}$$
$$\sigma_B \simeq 4.4 \times 10^6 \text{ newtons m}^{-2}$$

and that on the base of the plates is

$$\sigma_A \simeq 1.3 \times 10^6 \text{ newtons m}^{-2}$$
$$\sigma_B \simeq 2.0 \times 10^6 \text{ newtons m}^{-2}$$

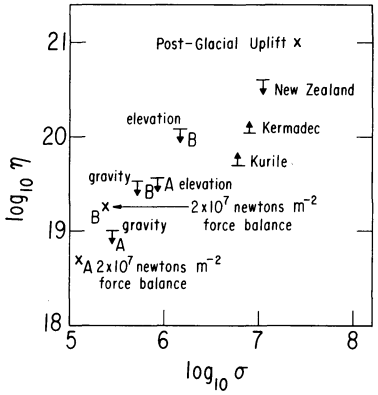


**Fig. 12.** Estimates of viscosity (kg $s^{-1}$ $m^{-1}$) of and stress (newtons $m^{-2}$) within a one layer mantle of constant viscosity (see text). Crosses mark estimated values, horizontal lines with arrows mark bounds; upper bounds if the arrow points downwards, lower if it points upward. *A* and *B* refer to the two plate models

It is, however, improbable that these values are sensible. The model requires large forces to be transmitted through the lithosphere beneath the trench. The stress involved is easily obtained from Figure 10, and is about $1.8 \times 10^8$ newtons $m^{-2}$. Since the lithosphere appears to be broken by normal faults in the region where it bends beneath the island arcs, this stress must be transmitted by friction. Since there is little evidence in favour of such large stresses being involved in earthquakes (see section 3) it seems more sensible to limit the stress to some value, and we choose $2 \times 10^7$ newtons $m^{-2}$ and then use the scaled dimensionless forces in Figures 4a and 7 to obtain the value of the viscosity which will allow the plate to move. This balance gives

$$\eta_A \simeq 5.5 \times 10^{18} \text{ kg s}^{-1} \text{ m}^{-1} \qquad \sigma_A \simeq 1.4 \times 10^5 \text{ newtons m}^{-2}$$
$$\eta_B \simeq 1.8 \times 10^{19} \text{ kg s}^{-1} \text{ m}^{-1} \qquad \sigma_B \simeq 2.4 \times 10^5 \text{ newtons m}^{-2}$$

which are shown in Figure 12. Since the total force on the plates must be zero these are estimates, not upper or lower bounds. Since the slab is broken and does not move with a uniform velocity we can no longer use the simple models to examine the total force balance. Under these conditions the buoyancy of the sinking slabs must be balanced locally by the pressure and shearing forces but these resistive forces cannot be estimated unless the velocity variation is known.

Figure 11 shows that the bottom 150 km of the slabs beneath the Kermadec and the Kurile arcs is in compression. The consumption rates are both around 80 mm $yr^{-1}$, and their bases are at 550 km and 620 km respectively. If we assume that the sinking rate is equal to the consumption rate we can use Figure 10 to obtain

$$\eta \gtrsim 1.1 \times 10^{20} \text{ kg s}^{-1} \text{ m}^{-1}, \qquad \sigma \gtrsim 8 \times 10^6 \text{ newtons m}^{-2}$$

for the Kermadec Arc and

$$\eta \gtrsim 5 \times 10^{19} \text{ kg s}^{-1} \text{ m}^{-1}, \qquad \sigma \gtrsim 6 \times 10^6 \text{ newtons m}^{-2}$$

for the Kurile Arc, where the stresses refer to the mean shear stress on the sides of the lower 150 km of the plate.

The last limits come from the existence of detached blocks. If we use the $u_z' = -2$ case with $V = 15\,\text{mm yr}^{-1}$ and require a block 150 km long to fall with a velocity of at least $30\,\text{mm yr}^{-1}$ (see above and Fig. 8), we require:

$$\eta \gtrsim 4 \times 10^{20}\,\text{kg s}^{-1}\,\text{m}^{-1}, \quad \sigma \gtrsim 1.1 \times 10^{7}\,\text{newtons m}^{-2}$$

This value of the viscosity is considerably greater than that obtained by Christoffel and Calhaem (1973) for New Zealand because they required the block to sink at $100\,\text{mm yr}^{-1}$ and be only 60 km in length.

The limits shown in Figure 12 are quite obviously incompatible. The viscosity required varies by two orders of magnitude. If the creep rate is a non-linear function of stress when the stress exceeds a certain value, estimated to be about 10 newtons $\text{m}^{-2}$ (Stocker and Ashby, 1973; Weertman, 1970) the problem becomes worse, since the effective viscosity is a decreasing function of shear stress, whereas Figure 12 requires the opposite. The only reasonable explanation for the failure of the model is that the viscosity of the mantle is not constant but increases with depth. The simplest model is then one which contains two layers, an upper layer with low viscosity which allows the plates to slide and a lower one of higher viscosity. Unfortunately two parameters are required to describe such a model, and for this reason it is no longer possible to obtain dimensionless forces valid for all viscosities as was done for the one layer model. Instead of carrying out extensive calculations with a wide variety of two layer models we chose to obtain approximate expressions for the forces on sinking slabs from the one layer calculations and only carry out a complete two layer calculation for the interior flow, where analytic expressions can be obtained. The estimates of the forces acting on the sinking slabs are little affected by the presence of a thin low viscosity layer.

### *Two-Layer Models*

We consider two models, model *C* has an upper layer 85 km thick, and in model *D* it is 8.5 km thick. Both can satisfy the observational constraints, though a model similar to *C* seems to us more plausible. We first estimate the viscosity $\eta_2$ of the lower layer assuming that no stress is transmitted through its upper surface, and then discuss the likely range of the viscosity of the upper layer.

Models of this type with thin low viscosity zones beneath the plates have been suggested by several authors (Anderson, 1962; Green, 1972; Wyllie, 1971) who believe the uppermost mantle to be partly molten. The existence of a fluid phase insufficient by itself to lower the viscosity. If, however, the liquid phase is in equilibrium with the solid, mass transfer may occur through the fluid and in this way dramatically lower the viscosity.

If the resistive forces are required to balance a total buoyancy of order $2 \times 10^{13}$ newtons $\text{m}^{-1}$ (Fig. 9), then

$$\eta \gtrsim 5 \times 10^{20}\,\text{kg s}^{-1}\,\text{m}^{-1} \qquad \sigma \gtrsim 1.1 \times 10^{7}\,\text{newtons m}^{-2}$$

for the Kermadec slab and

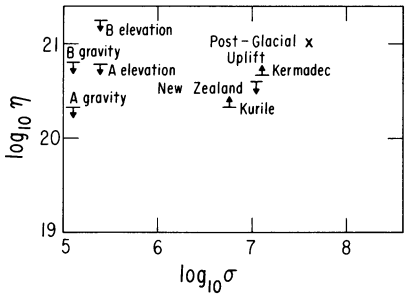


**Fig. 13.** Estimates of viscosity (kg $s^{-1}$ $m^{-1}$) of and stress (newtons $m^{-2}$) within the lower layer of a two layer model, *C* for the mantle. The symbols have the same meanings as in Figure 12. The estimates marked *A* and *B* are uncertain, and could be increased or decreased by at least a factor of 3

$$\eta \gtrsim 2.2 \times 10^{20} \text{ kg s}^{-1} \text{ m}^{-1} \qquad \sigma \gtrsim 6.6 \times 10^{6} \text{ newtons m}^{-2}$$

for the Kurile slab. The values of $\eta$ are somewhat larger than the one layer values principally because of the stress free condition which causes the contribution of the interior flow to $p_1$ to be small. The falling block gives values which are little affected by the free upper surface. These values are plotted in Figure 13 and are in substantial agreement with the value obtained from post-glacial uplift. It is not at once obvious why these values should agree. Clearly if the viscosity of the upper layer is sufficiently small the ice load will be compensated by movement of material within the upper layer (see Appendix) and produce a periferal bulge around the load. If this is not to occur then $\eta_2/\eta_1 \gtrsim 10^4$ for model *C* and $\gtrsim 10^6$ for model *D*. If, however, the above conditions are satisfied the low viscosity layer may become extremely hard to detect, especially when it is overlain by an elastic plate (Peltier, personal communication). The only effect of the upper layer is to alter the boundary condition on the upper surface of the lower layer. In the absence of a low viscosity layer the tangential velocity due to the ice load must vanish at the base of the plate, whereas when a low viscosity layer is present the shear stress vanishes instead. However, if the lower layer is a half space, both boundary conditions are satisfied by a stream function

$$\psi = c(kz - 1)\, e^{kz} \sin kx$$

where $c$ is a constant, and $k$ is the wavenumber, and therefore post-glacial uplift cannot distinguish between the two boundary conditions, and in both cases determines the viscosity of the lower layer.

The other apparent difficulty involves the rigid boundary imposed at a depth of 700 km. Peltier and Andrews (1976) could not account for the post-glacial uplift without permitting flow to occur below this depth. If, however, the rigid region is as thin as McKenzie and Weiss (1975) believed, it would not influence the surface motion but would still prevent the return flow penetrating the lower mantle.

*The Upper Layer*

We wish the upper layer to decouple the plate motions from the motions below, but it must not channel the horizontal flow. If it did so this would be apparent

in the post-glacial uplift observations. Another observation which excludes this possibility is the observed correlation between the depth of the ocean and gravity anomalies (Sclater et al., 1975). If normal stresses could not be transmitted to the base of the plate then its upper surface would be an equipotential after the age corrections had been made. Since the ocean surface is an equipotential, the corrected depth would be constant (McKenzie, 1977). This is not the case. Therefore the viscosity of the upper layer must be sufficiently small to decouple the plate motions from the lower layer, but large enough to prevent large horizontal mass fluxes within it. These conditions cannot be satisfied if the layer is much thicker than 85 km. The limits for model $C$ are

$$2\times 10^2 \lesssim \eta_2/\eta_1 \lesssim 10^3$$

and for $D$

$$10^3 \lesssim \eta_2/\eta_1 \lesssim 10^5.$$

If we take $\eta_2$ to be $2.5\times 10^{20}$ kg m$^{-1}$ s$^{-1}$ and $\eta_1 = 5\times 10^{17}$, $2.5\times 10^{17}$ for models $C$ and $D$, respectively, we satisfy these two constraints. Using the expressions in the Appendix, and including the sliding force we find that the force required to maintain the surface plate motions corresponds to stresses within the plates at island arcs of

$$\sigma_A \simeq 2.6\times 10^7 \text{ newtons m}^{-2}$$
$$\sigma_B \simeq 7.9\times 10^6 \text{ newtons m}^{-2}$$

in model $C$ for the two plates and

$$\sigma_A \simeq 3.2\times 10^7 \text{ newtons m}^{-2}$$
$$\sigma_B \simeq 9.7\times 10^6 \text{ newtons m}^{-2}$$

for model $D$. It is therefore possible to maintain the plate motions by frictional forces transmitted across faults, and also to provide enough resistance to permit the upper part of some sinking slabs to be in tension. One further condition must be satisfied. There is no evidence that the heat flow through old parts of plates depends on the spreading rate, and therefore shear stress heating should not make an important contribution to the surface heat flux. The total contribution from this source for plate $A$ using model $C$ is about $8\times 10^{-4}$ Watts m$^{-2}$, and for model $D$ is about $7\times 10^{-4}$ Watts m$^{-2}$. Both are less than 2% of the surface heat flux. It is clear from this discussion that the difficulties faced by a one-layer model are removed if a thin low viscosity layer is present beneath the plates.

## 5. The Driving Force for Plate Motions

In the last section we have argued that geophysical observations require a large contrast in viscosity within the mantle. A high viscosity lower layer is required to account for the post-glacial uplift data and for the fault plane solutions for deep earthquakes. However, unless the surface motions are decoupled from this

lower layer by a low viscosity region, long wavelength gravity anomalies or residual depth variations are produced whose magnitude is about two orders of magnitude larger than those observed. We argued that a model with a thin low viscosity layer beneath the plates could reconcile the differences between the different estimates of viscosity, but it is also important to discuss whether the model is compatible with the extensive knowledge of plate motions.

The two plate models considered above both contain sinking slabs, and therefore buoyancy forces from density contrasts beneath trenches are available to maintain the motions. For this reason these models closely resemble that of Elsasser (1969), who suggested that this buoyancy force could drive all observed motions. One of the principal objections to this idea was that many large plates, such as Eurasia, America, Africa and Antarctica are in relative motion (McKenzie, 1969). At first sight this objection is overcome by the convective forces available from ridge pushing. Unfortunately such forces are available only if spreading is already taking place, and therefore they cannot break an existing plate. Since it seems likely that the separation of both North America and Eurasia and of South America and Africa started when no large sinking slabs were attached to any of these plates, another source of work is required. One possibility is that the decoupling layer is absent beneath shield regions, and hence that continents are strongly coupled to flows in the mantle. Another is the sliding force discussed in section 2, given by Eq. (18). This force exists because convection in the lower layer lifts the plate on top. Sclater et al. (1975) showed that parts of the North Atlantic were up to 1 km shallower than expected from their age. Even when shear stresses do not act on the base of the plates, such an elevation produces a stress of about $2.3 \times 10^7$ newtons $m^{-2}$ which is comparable to that expected from a sinking slab. Large positive elevations exist in the North Atlantic and South West Indian Ocean which could maintain the relative motions of North America, Eurasia, Africa and Antarctica, but it is less easy to understand why the South Atlantic is spreading faster than any of the other ridges between non-subducting plates. Either mechanism can account for the formation of new plate boundaries, since the stress involved is comparable to that involved in earthquakes.

It is encouraging that there do not appear to be any major conflicts between the simple models considered above and the geophysical observations. One of the few obvious problems is in the Eastern Pacific, with the Cocos plate. The distance between the two ridges and the Middle America trench is only about 1000 km, and therefore the pressure difference required to drive the return flow is much less than that for large plates such as the Pacific. Probably for this reason the sinking slab beneath Central America is in tension. Despite the lack of resistive forces the Cocos plate does not appear to be accelerating as the length of the sinking slab increases. Any such acceleration would show clearly on the magnetic profiles across the Galapagos Rift. Perhaps the explanation is that the buoyancy of the sinking slab is smaller than elsewhere because the plate now being consumed is relatively young and warm.

The two-layer model implies that the velocities of plate motion are considerably greater than those within the lower layer. If melting spots are the surface expression of structures in the lower layer then their relative motion should be slow compared to the plate velocities, as Minster et al. (1974) have demon-

strated. Therefore this model is consistent with the observations that Morgan (1971, 1972) has argued require the existence of plumes of hot rising material extending to greater depths.

Our models have various important shortcomings which prevent them from being used for detailed calculations using the observed plate geometries. We have assumed that all the motions are two dimensional, and obviously the observed motions are strongly three dimensional. We have taken all slabs to be vertical and to be stationary with respect to the lower boundary of the fluid layer. Since the buoyancy force normal to a dipping slab must be balanced by a pressure difference across the slab, non-vertical slabs make a large contribution to the pressure field. Relative motion between the slab and the lower boundary must also make an important contribution to the pressure field. Perhaps realistic calculations will be possible, though they will not be straightforward because of resolution problems. Hager and O'Connell (1977) have recently calculated the three-dimensional flow in the earth's interior which is consistent with the observed surface velocities, but they take no account of the contribution that the sinking slabs make to the flow through their rigidity and their buoyancy. It seems likely that both effects are important.

## Conclusions

The most important result we have obtained is that several uncontroversial geophysical observations combined with an idealized model of plate dynamics, impose important constraints on the form of mantle convection. In particular a constant viscosity mantle is ruled out by the magnitude of the long wavelength gravity and residual depth anomalies and the stress state within the sinking slabs. However, a model with two layers of widely different viscosity can satisfy these and other observations, but only if the viscosity of the upper layer is a factor of about 500 less than that of the lower. Furthermore, the thickness of the upper layer cannot be greater than about 100 km, and may be thinner. Despite the decoupling which such a low viscosity region produces, mantle convection can maintain plate motions and form new plate boundaries. Provided the upper layer is thin, such a two-layer model does not appear to be in conflict with other observations such as post-glacial uplift, and has been in fact already proposed to account for isostasy (Fisher, 1881) and the attenuation of seismic waves (Anderson, 1962). The low viscosity may be produced by a very small fraction of partial melt believed to be present in the low velocity layer beneath the plates (Green, 1972).

Our investigation has demonstrated the importance of the pressure perturbation due to the flow. The pressure contribution controls the stress state within the sinking slabs, the surface deformation and the gravity anomaly associated with the return flow from trenches to ridges. More information can be obtained about this pressure field from focal mechanisms of earthquakes within slabs which extend to depths of 400 km or less (McKenzie, 1976).

Our model is consistent with the existence of two scales of flow within the mantle. Because the plate motions are decoupled from most of the mantle

below, the small-scale flow is more likely to consist of three-dimensional time dependent motions than two-dimensional rolls. We have principally discussed that part of the large-scale flow which is associated with plate motions, but it is not possible to maintain the observed long wavelength gravity anomalies by such flow. A large-scale circulation not directly associated with the mass fluxes generated by plate motions must also exist. The energetics and stability of this flow are not yet understood, and can only be investigated by a model which takes account of buoyancy forces within the fliud.

Our model is also consistent with the results of Forsyth and Uyeda (1975) and of Chapple and Tullis (1977) who used the observed plate motions to estimate the importance of a variety of forces driving and resisting plate motions. Both pairs of authors found similar results: The large driving forces due to the sinking slabs are resisted locally and are not communicated to the plate which is being consumed. The form that this resistance takes differs in the two models because the authors formulate the problem in slightly different ways. Forsyth and Uyeda find that most of the buoyancy force is balanced by stresses on sides and ends of the slabs. Chapple and Tullis do not allow for such forces and find that the buoyancy force is balanced by forces between the converging plates, and they then balance the reaction on the island arc by a local driving force. All the other forces in both models are considerably smaller, a result which requires decoupling of the plate motions from those of the mantle below. However, neither model was concerned with the physical processes which produced the resistive forces. The agreement between our results and the two models is very encouraging, especially because our approach is so different.

*Acknowledgements.* We thank Barry Parsons for many helpful suggestions. This work forms part of a general investigation of mantle convection at Cambridge, supported by the Natural Environmental Research Council. It was also in part supported by a National Science Foundation Grant, NSF EAR-75 17170.

F. Richter thanks the John Simon Guggenheim Foundation for a fellowship which supported his visit to Cambridge.

## Appendix

The interior solution to the two-layer model shown in Figure 14 is easily obtained, though the algebra is tedious. If $d_2$ and $\eta_2$ are used to reduce the equations to dimensionless form and

$$M=\eta_2/\eta_1, \quad r=d_1/d_2, \quad t'=t/d_2$$

then

$$\frac{dp_1'}{dx'}=-\frac{6\{2t'(1+Mr)+(1+2r+Mr^2)\}}{1+4Mr+6Mr^2+4Mr^3+M^2r^4}. \tag{A.1}$$

When $M\to\infty$ (A.1) becomes

$$\frac{dp_1'}{dx'}=-\frac{6(2t'+r)}{Mr^3}.$$

Hence

$$\frac{dp_1}{dx}=-\eta_1 V\frac{6(2t+d_1)}{d_1^3} \tag{A.2}$$

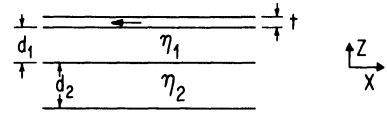


**Fig. 14.** Two-layer model with different viscosity $\eta$ in each layer

Thus $dp_1/dx$ is independent of both $\eta_2$ and $d_2$ and hence the properties of the lower layer. This behaviour occurs because the return flow occurs entirely within the upper layer, as can be seen either by examining the mass flux or by comparing (A.2) with (13). Hence this is not the limit corresponding to (14) which allows the motion of the plate to decouple from that of the lower layer. To obtain this limit we require $M \to \infty$ and $r \to 0$, while $Mr \to \infty$ and $Mr^2 \to 0$ giving

$$\frac{dp_1'}{dx'} \to -3t' \tag{A.3}$$

In this limit no stress is transmitted across the upper layer, but the return flow is restricted to the lower layer.

The expression for the dimensionless shear stress $\sigma'$ on the base of the plate may be obtained from (A.1)

$$\sigma' = \left\{1 - \frac{1}{2}\frac{dp_1'}{dx'}(Mr^2 + 2r + 1)\right\} \Big/ (1 + Mr) \tag{A.4}$$

The fraction $f$ of the return flow taking place in the upper layer is

$$f = \frac{r}{2t(1+Mr)}\left\{2 + Mr + \frac{1}{6}\frac{dp_1'}{dx'} Mr(3 + 4r + Mr^2)\right\} \tag{A.5}$$

The average dimensionless viscous dissipation $\Phi_1'$ in the upper layer is

$$\Phi_1' = M\left\{B^3 - \left(B - \frac{dp_1'}{dx'}\right)^3\right\} \Big/ 3r\frac{dp_1'}{dx'} \tag{A.6}$$

and in the lower layer

$$\Phi_2' = \left\{\left(B + \frac{dp_1'}{dx'}\right)^3 - B^3\right\} \Big/ 3\frac{dp_1'}{dx'} \tag{A.7}$$

where

$$B = \left\{1 - \frac{1}{2}\frac{dp_1'}{dx'}(1 - Mr^2)\right\} \Big/ (1 + Mr) \tag{A.8}$$

The dimensionless velocity $u_x'$ at the interface is

$$u_x' = \left\{1 + \frac{1}{2}\frac{dp_1'}{dx'} Mr(1 + r)\right\} \Big/ (1 + Mr) \tag{A.9}$$

## References

Anderson, D.L.: The plastic layer of the earth's mantle. Sci. Amer. July 1962, pp. 52–59, 1962

Chapple, W.M., Tullis, T.E.: Evaluation of the forces that drive the plates. J. Geophys. Res. **82**, 1967–1984, 1977

Christoffel, D.A., Calhaem, I.M.: Upper mantle viscosity determined from Stokes' Law. Nature Phys. Sci. **243**, 51–52, 1973

Davies, G.F.: Whole mantle convection and plate tectonics. Geophys. J. Roy. Astron. Soc. **49**, 459–486, 1977a

Davies, G.F.: Viscous mantle flow under moving lithospheric plates and under subduction zones. Geophys. J. Roy. Astron. Soc. **49**, 557–563, 1977

Elsasser, W.M.: Convection and stress propagation in the upper mantle. In: The Application of Modern Physics to the Earth and Planetary Interiors, S.K.: Runcorn, ed.: pp. 223–246. New York: Interscience 1969

Fisher, O.: Physics of the Earth's Crust. London: MacMillan 1881

Forsyth, D., Uyeda, S.: On the relative importance of the driving forces of plate motion. Geophys. J. Roy. Astron. Soc. **43**, 163–200, 1975

Fukao, Y.: Source process of a large deep-focus earthquake and its tectonic implications. – The western Brazil earthquake of 1963. Phys. Earth Planet. Inter. **5**, 61–76, 1972

Fukao, Y.: Thurst faulting at a lithospheric plate boundary: The Portugal earthquake of 1969. Earth Planet. Sci. Lett. **18**, 205–216, 1973

Gaposchkin, E.M.: Earth's gravity field to the eighteenth degree and geocentric coordinates for 204 stations from satellite and terrestrial data, J. Geophys. Res. **79**, 5377–5411, 1974

Green, D.H.: Magmatic activity as the major process in the chemical evolution of the earth's crust and mantle. In. The Upper Mantle, A.R. Ritsema, ed. pp. 47–71, Amsterdam: Elsevier 1972

Hager, B.H., O'Connell, R.J.: Benioff zone dip angles and flow driven by moving planes. Trans. Am. Geophys. Union **58**, 499 (abstract), 1977

Hewitt, J.M., McKenzie, D.P., Weiss, N.O.: Dissipative heating in convective flows. J. Fluid Mech. **68**, 721–738, 1975

Isacks, B.L., Molnar, P.: Distribution of stresses in the descending lithosphere from a global survey of focal-mechanism solutions of mantle earthquakes. Rev. Geophys. Space Phys. **9**, 103–174, 1971

Isacks, B.L., Oliver, J., Sykes, L.R.: Seismology and the new global tectonics. J. Geophys. Res. **73**, 5855–5899, 1968

Kanamori, H.: Synthesis of long-period surface waves and its application to earthquake source studies. – Kurile Islands earthquake of October 13, 1963. J. Geophys. Res. **75**, 5011–5027, 1970a

Kanamori, H.: The Alaskan earthquake of 1964: radiation of longperiod surface waves and source mechanism. J. Geophys. Res. **75**, 5029–5040, 1970b

Kanamori, H.: Focal mechanism of the Takachi-Oki earthquake of May 16, 1968: contortion of the lithosphere at a junction between two trenches, Tectonophysics **12**, 1–13, 1971

Lerch, F.J., Wagner, C.A., Richardson, J.A., Brownd, J.E.: Goddard earth models (5 and 6). Goddard Space Flight Centre report no. x-921-74.145, 1974

McKenzie, D.P.: The influence of the boundary conditions and rotation on convection in the earth's mantle. Geophys. J. Roy. Astron. Soc. **15**, 457–500

McKenzie, D.P.: Speculations of the causes and consequences of plate motions. Geophys. J. Roy. Astron. Soc. **18**, 1–32, 1969

McKenzie, D.P.: The orientation of the stress within sinking slabs. Earth Planet. Sci. Lett. **31**, 305–307, 1976

McKenzie, D.P.: Surface deformation, gravity anomalies and convection. Geophys. J. Roy. Astron. Soc. **48**, 211–238, 1977

McKenzie, D.P., Roberts, J.M., Weiss, N.O.: Convection in the earth's mantle: towards a numerical simulation. J. Fluid Mech. **62**, 465–538, 1974

McKenzie, D.P., Weiss, N.O.: Speculations on the thermal and tectonic history of the earth. Geophys. J. Roy. Astron. Soc. **42**, 131–174, 1975

Mikumo, T.: Focal process of deep and intermediate earthquakes around Japan as inferred from long-period *P* and *S* waveforms. Phys. Earth Planet. Inter. **6**, 293–299, 1972

Minister, J.B., Jordan, T.H., Molnar, P., Haines, E.: Numerical modelling of instantaneous plate tectonics. Geophys. J. Roy. Astron. Soc. **36**, 541–576, 1974

Molnar, P., Atwater, T., Mammerickx, J., Smith, S.M.. Magnetic anomalies, bathymetry and the tectonic evolution of the South Pacific since the late Cretaceous. Geophys. J. Roy. Astron. Soc. **40**, 383–420, 1975

Molnar, P., Tapponnier, P.. Cenozoic tectonics of Asia: effects of a continental collision. Science **189**, 419–426, 1975

Morgan, W.J.: Convection plumes in the lower mantle. Nature **230**, 42–43, 1971

Morgan, W.J.: Deep mantle convection plumes and plate motions. Bull. Amer. Ass. Petrol. Geol. Bull. **56**, 203–213, 1972

O'Connell, R.J.: On the scale of mantle convection. Tectonophysics **38**, 119–136, 1977

Parsons, B., Sclater, J.G.: An analysis of the variation of ocean floor bathymetry and heat flow with age. J. Geophys. Res. **82**, 803–827, 1977

Pekeris, C.L.: Thermal convection in the interior of the earth, Monthly Notices Roy. Astron. Soc. Geophys. Suppl. **3**, 343–367, 1935

Peltier, W.R., Andrews, J.T.: Glacial-isostatic adjustment I: the forward problem. Geophys. J. Roy. Astron. Soc. **46**, 605–646, 1976

Prothero, W.A., Reid, I., Reickle, M.S., Brune, J.N.: Ocean bottom seismic measurements on the East Pacific Rise and Rivera Fracture Zone. Nature **262**, 121–124, 1976

Rayleigh, C.B., Healy, J.H., Bredehoeft, J.D.: Faulting and crustal stress at Rangely, Colorado. In: Flow and Fracture of Rocks, H.C. Heard et al., ed.: A.G.U. monograph **16**, pp. 275–284, 1972

Richter, F.M.: Dynamical models for sea-floor spreading. Rev. Geophys. Space Phys. **11**, 223–287, 1973a

Richter, F.M.: Convection and the large scale circulation of the mantle. J. Geophys. Res. **78**, 8735–8745, 1973b

Richter, F.M.: On the driving mechanism of plate tectonics. Tectonophysics **38**, 61–88, 1977

Richter, F.M., Parsons, B.: On the interaction of two scales of convection in the mantle. J. Geophys. Res. **80**, 2529–2541, 1975

Sbar, M.L., Sykes, L.R.: Contemporary compressive stress and seismicity in eastern North America: an example of intra-plate tectonics. Bull. Geol. Soc. Am. **84**, 1861–1882, 1973

Schubert, G., Turcotte, D.L.: One-dimensional model of shallow-mantle convection. J. Geophys. Res. **77**, 945–951, 1972

Sclater, J.G., Lawver, L.A., Parsons, B.: Comparison of long-wavelength residual elevation and free air gravity anomalies in the North Atlantic and possible implications for the thickness of the lithospheric plate. J. Geophys. Res. **80**, 1031–1052, 1975

Stocker, R.L., Ashby, M.F.: On the rheology of the upper mantle, Rev. Geophys. Space Phys. **11**, 391–426, 1973

Weertman, J.: The creep strength of the earth's mantle. Rev. Geophys. Space Phys. **8**, 145–168, 1970

Weidner, D.J., Aki, K.: Focal depth and mechanism of mid-ocean ridge earthquakes. J. Geophys. Res. **78**, 1818–1831, 1973

Wu, F., Kanamori, H.: Source mechanism of February 4, 1965, Rat Island earthquake. J. Geophys. Res. **78**, 6082–6092, 1973

Wyllie, P.J.: The Dynamic Earth. New York: J. Wiley & Sons 1971

Wyss, M.: Apparent stresses of earthquakes on ridges compared to apparent stress of earthquakes in trenches. Geophys. J. Roy. Astron. Soc. **19**, 479–484, 1970

Wyss, M., Molnar, P.: Source parameters of intermediate and deep focus earthquakes in the Tonga Arc. Phys. Earth Planet. Inter. **6**, 279–292, 1972

Received August 1, 1977 / Revised Version February 10, 1978